Novel insights into the development of the avian nasal cavity

ZAHRA ALBAWANEH, RAANA ALI, AND JOHN ABRAMYAN*
Department of Natural Sciences, University of Michigan-Dearborn, Dearborn, Michigan

ABSTRACT

In embryonic amniotes, patterning of the oral and nasal cavities requires bilateral fusion between craniofacial prominences, ensuring an intact primary palate and upper jaw. After fusion has taken place, the embryonic nasal cavities open anteriorly through paired external nares positioned directly above the fusion zones and bordered by the medial nasal and lateral nasal prominences. In this study, we show that in the chicken embryo, the external nares initially form as patent openings but only remain so for a short period of time. Soon after the nasal cavities form, the medial nasal and lateral nasal prominences fuse together in stage 29 embryos, entirely closing off the external nares for a substantial portion of embryonic and fetal development. The epithelium between the fused prominences is then retained and eventually develops into a nasal plug that obstructs the nasal vestibule through the majority of the fetal period. At stage 40, the nasal plug begins to break down through a combination of cellular remodeling, apoptosis, as well as non-apoptotic necrosis, leading to completely patent nasal cavities at hatching. These findings place chickens in a category with several species of nonavian reptiles and mammals (including humans) that have been found to develop a transient embryonic nasal plug. Our findings are discussed in the context of previously reported cases of nasal plugs as part of normal embryonic development and provide novel insight into the craniofacial development of a key model organism in developmental biology. Anat Rec, 00:000–000, 2019. © 2019 American Association for Anatomy

Key words: chicken; craniofacial; nasal cavity; nasal plug; prominences

1. INTRODUCTION

The components of embryonic craniofacial development are remarkably conserved across amniotes (Abramyan & Richman, 2015; Abramyan, Thivichon-Prince, & Richman, 2015). The face is assembled from a set of craniofacial prominences that grow out bilaterally and fuse together toward the front of the face. The lower jaw forms from paired mandibular prominences (Richman & Tickle, 1989; Wedden, 1987). The upper jaw arises from a frontonasal mass (or frontonasal prominence), paired maxillary prominences, paired lateral nasal prominences, and paired medial nasal prominences (which arise from the frontonasal mass) (Figure 1); (Abramyan et al., 2015; Will & Meller, 1981; Yee & Abbott, 1978). In mammals, the maxillary prominences fuse with the medial nasal prominences to form an intact upper jaw and nasal cavities (Jiang, Bush, & Lidral, 2006). In avian embryos, the

Grant sponsor: National Center for Research Resources; Grant number: S10RR026475-01; Grant sponsor: National Institute of Arthritis and Musculoskeletal and Skin Diseases; Grant number: P30 AR069620; Grant sponsor: University of Michigan-Dearborn.

*Correspondence to: John Abramyan, Department of Natural Sciences, University of Michigan-Dearborn, 114 SFC Bldg. 4901 Evergreen Rd. Dearborn, MI 48128.
Email: abramyan@umich.edu

Received 20 October 2019; Revised 17 November 2019; Accepted 18 November 2019.
DOI: 10.1002/ar.24349
Published online 00 Month 2019 in Wiley Online Library (wileyonlinelibrary.com).

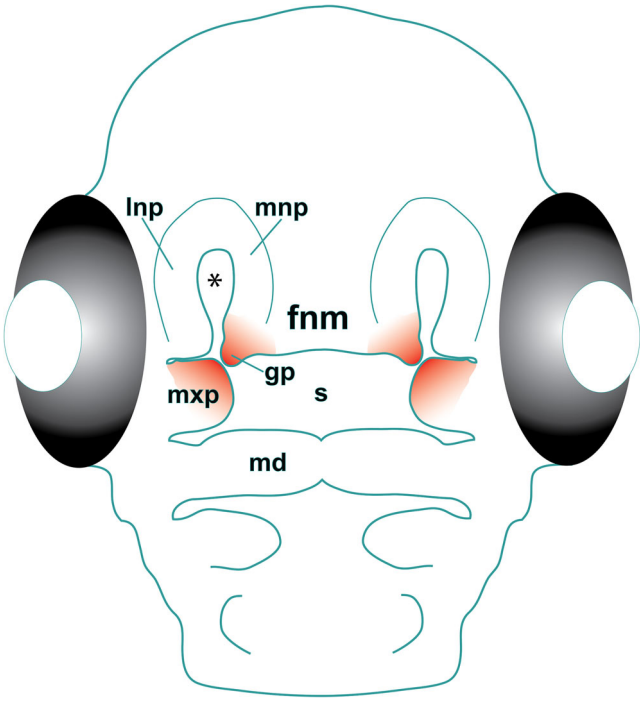

Fig. 1. Depiction of a stage 28 chicken embryo with red shading highlighting the regions of fusion between the maxillary prominences and the globular processes of the frontonasal mass. Asterisk indicates an open nasal cavity. fnm, frontonasal mass; gb, globular process; lnp, lateral nasal prominence; md, mandibular prominence; mnp, medial nasal prominence; mxp, maxillary prominence; s, stomodeum

medial nasal prominences are often poorly defined as distinct structures since they do not develop a deep midsagittal groove between them. Therefore, the avian maxillary prominence is typically described as fusing with the globular process of the frontonasal mass, caudal to the medial nasal prominence proper (Tamarin, Crawley, Lee, & Tickle, 1984) (Figure 1). Fusion between the globular processes and the maxillary prominences completes patterning of the primary palate (anterior-most region of the palate), upper jaw, as well as upper lip and nasal cavities (described in detail by Abramyan & Richman, 2015 and Abramyan et al., 2015). Despite minor differences, the extraordinary conservation of embryonic craniofacial patterning allows for extensive use of both mouse and chicken in characterization of human craniofacial development and pathology (Abramyan & Richman, 2018; Bedell et al., 1997, 1997; Dodgson & Romanov, 2004).

As the upper jaw forms through fusion of the prominences, the nasal and oral cavities separate from each other and become distinct structures. Externally, the openings to the nasal cavities are visible as paired external nares above the mouth in mammals and sauropsids, the clade that includes extant reptiles and birds. Internally, the nasal cavities connect with the oral cavity and the pharynx through paired internal openings called choanae (Jankowski, 2011; Kim, Park, Kim, & Yoon, 2004). The nasal cavities themselves may be divided into three anatomical compartments arranged anterior to posterior: the rostral nasal vestibule, the nasal cavity proper, and the nasopharyngeal duct (Parsons, 1959, 1970; Witmer, 1995). In birds, the vestibule is particularly expanded, while the nasopharyngeal duct is highly reduced or often absent (Witmer, 1995). Within the aforementioned compartments, amniotes develop nasal conchae (turbinals), which can range in number from one in squamates to a row of conchae of variable number in mammals and birds (Hillenius, 1994; Van Valkenburgh, Smith, & Craven, 2014). Birds develop three sets of conchae. The rostral nasal conchae (anterior turbinals) develop in the vestibule, while the middle and caudal conchae (middle and posterior turbinals) form in the respiratory and olfactory portions of the nasal cavity proper (Witmer, 1995).

In neonatal amniotes, the nasal cavities have to be patent since they are utilized for a variety of postnatal functions including respiration, olfaction, vocalization, air filtration, heat dissipation, as well as warming of inhaled air (Dahl & Mygind, 1998; Hillenius, 1994). However, during embryonic development, studies have found that nasal cavities are often transiently obstructed by tissue, and must recanalize prior to hatching or birth. Obstruction of the nasal passages can occur via blockage of the choanae, external nares, or both (Buchtova, Boughner, Fu, Diewert, & Richman, 2007; Diewert & Shiota, 1990). The closure and subsequent reopening of the mammalian choana is well studied due to its association with choanal atresia, a condition that co-occurs with a number of craniofacial syndromes, where the choanae fail to reopen and thus nasal respiration is obstructed (Kurosaka, 2019). Obstruction of the external nares, however, has received relatively less attention and is thought to occur through the formation of transient epithelial nasal plugs, both in reptiles (Buchtova et al., 2007; Howes & Swinnerton, 1901) and mammals (Alomaisi, El-Ghazali, Nosseur, Ahmed, & Konsowa, 2018; Bollert & Hendrickx, 1971; Kim et al., 2004; Nishimura, 1993; Wassif et al., 2001), with no recorded cases in avian embryos.

The purpose of this study was to closely examine the formation of the avian nasal cavity, with the use of the chicken embryo as a model. We were specifically interested in determining whether a nasal plug forms in this group at any point during embryonic and fetal stages of development. Surprisingly, this aspect of development in the chicken embryo appears to have gone unobserved, despite the fact that they have been used extensively as a model of developmental biology and embryology for over a century (Abramyan & Richman, 2018; Kain et al., 2014). In this study, we applied a combination of methods including X-ray micro-computed tomography (microCT) (Craven et al., 2007; Rossie, 2006; Rowe, Eiting, Macrini, & Ketcham, 2005), as well as traditional paraffin histology and tests for cellular apoptosis, to characterize the shape and structure of developing nasal cavities in the chicken embryo. We expect our findings to further the potential of the chicken embryo as a model organism for the study of human craniofacial development and pathology.

2. MATERIALS AND METHODS

2.1 Embryo acquisition and staging

Animal work was performed according to guidelines from the University of Michigan Animal Care and Use

program. Fertile chicken (*Gallus gallus*) eggs were obtained from the Michigan State University Poultry Teaching & Research Center, incubated in our laboratory at 38.0°C, and staged according to Hamburger and Hamilton (1951) (Table 1). At Day 2.5 of incubation (stage 15), eggs were windowed using standard procedures. Upon reaching stages required for various analyses, specimens were harvested and placed in cold 1× phosphate-buffered saline (PBS) and fixed in 4% paraformaldehyde (PFA)/PBS overnight, followed by dehydration in ethanol (EtOH) concentration series up to 70% for long term storage. Animals at stage 34 and above were first decapitated in ovo before harvesting.

2.2 MicroCT scanning conditions

There are a number of contrasting agents currently used to stain soft tissue for microCT (Gignac et al., 2016). In testing both phosphomolybdic acid (PMA) and iodine potassium iodide (IKI or Lugol's solution) in embryos of various stages, we found that PMA provided the best contrast, highest penetrance, and reduced side-effects (e.g., tissue shrinkage) in embryos younger than stage 30, while IKI was a better stain for stage 34 and stage 38 specimens. Fixed specimens in 70% ethanol were transferred to IKI or PMA for staining and subsequent scanning. Stage 28–29 specimens were stained with 1% PMA for 4 days. Afterward, they were embedded in 0.75% agarose for scanning. Stage 34 specimens were stained with 5% IKI for 4 days with one replacement at Day 2 and scanned in 75% ethanol. Specimens were scanned in a 19 mm diameter specimen holder, over the entirety of the head using a μCT100 Scanco Medical microCT system (Bassersdorf, Switzerland). Scan settings were voxel size 10 μm, 70 kVp, 114 μA, 0.5 mm AL filter, integration time of 500 ms, and 1,500 projections. Stage 38 specimens were stained with 10% IKI for 6 days, with replacement every 2 days, and scanned in 25% ethanol. Specimens were then placed in a 34 mm diameter specimen holder and scanned over the entirety of the head using a μCT100 Scanco Medical microCT system (Bassersdorf, Switzerland). Scan settings were voxel size 12 μm, 70 kVp, 114 μA, 0.5 mm AL filter, integration time of 500 ms, and 1,500 projections.

2.3 Volume rendering and segmentation

3D volume rendering was performed in MicroView (open-source software, Parallax Innovations Inc., Ilderton, ON, Canada). MicroCT scan .vff files were uploaded to MicroView, reoriented and cropped as needed. Files were then saved as .vtk files and uploaded to 3D Slicer version 4.2.2 (open-source software, http://www.slicer.org) for segmentation. Figures were compiled in Adobe Photoshop and Adobe Illustrator (Adobe Systems Inc., San Jose, CA).

TABLE 1. Stages and number of specimens used

Stage	MicroCT	Histology	Total	Figure
Stage 28	6	5	11	Figure 2
Stage 29	6	6	12	Figures 2 and 3
Stage 34	4	0	4	Figure 4
Stage 38	4	0	4	Figure 4
Stage 39	0	3	3	Figures 5 and 6
Stage 40	0	3	3	Figures 5 and 6
Stage 41	0	3	3	Figures 5, 6, and 7
Stage 42	0	4	4	Figures 5, 6, and 7
Stage 43	0	3	3	Figures 5, 6, and 7
Stage 44	0	3	3	Figure 5

Specimens used for histology also used for DAPI/TUNEL.

2.4 Histology

Different samples were used for histology and microCT in order to avoid unintended effects on tissue morphology such as shrinkage due to PMA or IKI staining. Embryos were harvested and fixed in 4% PFA overnight, followed by dehydration in an ethanol concentration series up to 70%. Stage 32 and above specimens were decalcified in Morse's solution for up to 1 week. Specimens were then embedded in paraffin, sectioned into 7 μm slices and mounted on slides. Sections were stained with picrosirius red to highlight skeletal and soft tissue and Alcian blue to highlight cartilage (Buchtova et al., 2007). Bright-field images were captured using a Nikon Eclipse E800 microscope equipped with a CoolSNAP-EZ CCD camera (Photometrics, Tucson, AZ) and NIS-Elements BR v. 4.12.01 software (Nikon, Melville, NY).

2.5 DAPI staining and TUNEL assay

Sections from specimens prepared for histological analysis were also utilized for 4′ 6-diamidino-2-phenylindole (DAPI) staining, as well as terminal deoxynucleotide transferase dUTP nick end labeling (TUNEL) analysis. TUNEL was performed with the ApopTag Fluorescein *In Situ* Apoptosis Detection Kit (EMD Millipore, Billerica, MA - S7110). Nuclei were stained with DAPI using Vectashield mounting medium for fluorescence with DAPI (Vector Laboratories, Burlingame, CA). Fluorescence images were captured using a Nikon Eclipse Ts2R inverted microscope (Nikon) equipped with a CoolSNAP Dyno monochrome CCD camera (Photometrics) and NIS-Elements BR v. 5.02 software (Nikon).

3. RESULTS

According to our findings, nasal cavity formation in the avian embryo may be divided into three phases. Phase 1 describes the period immediately after the fusion of the primary palate, where we observed a second fusion event between the medial nasal and lateral nasal prominences. Phase 2 involves the establishment of a nasal plug in the nasal vestibule and the formation of nasal conchae. Phase 3 focuses on the cellular processes involved in recanalization of the nasal vestibule, resulting in patent nasal cavities prior to hatching. These three sequential phases describe a developmental arc consisting of formation, establishment, and breakdown of nasal plugs in the chicken embryo.

3.1 Phase 1: Fusion of external nares (stages 28–29)

Isosurface renderings of stage 28 chicken embryos reveal the establishment of open external nares after initial fusion between the maxillary prominence and the globular process of the frontonasal mass (Figure 2a,a′—black arrowheads). With the transition to stage 29, the fusion zone expands (Figure 2b,b′—black arrowheads),

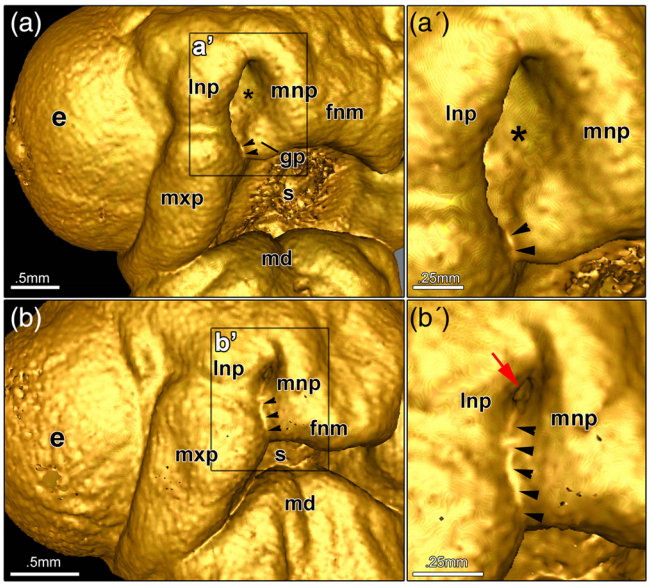

Fig. 2. MicroCT reconstructions of stage 28 and stage 29 chicken embryos exhibit differences in the degrees of external naris opening. Stage 28 specimens reveal open external naris (asterisk) and a relatively smaller region of fusion (black arrowheads) when the globular process and maxillary prominence first fuse (a, a′). Stage 29 specimens reveal an expanded region of fusion (black arrowheads) (b, b′), with a small opening to the nasal cavity visible at the cranial end (red arrow) (b′). e, eye; fnm, frontonasal mass; gp, globular process of the frontonasal mass; lnp, lateral nasal prominence; md, mandibular prominence; mnp, medial nasal prominence; mxp, maxillary prominence; s, stomodeum

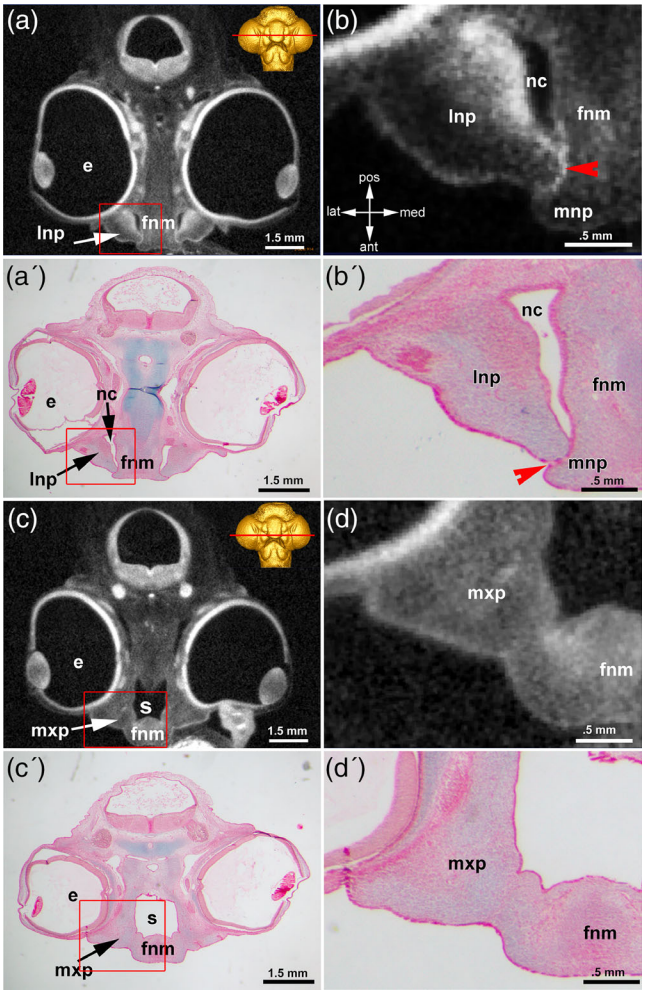

Fig. 3. Corresponding microCT slices and paraffin histological sections in the transverse plane of stage 29 embryo comparing fusion of the external naris and primary palate. Fused nasal prominences reveal retained epithelial seam between the lateral and medial nasal prominences (a-b′—red arrowhead). Sections through the newly fused primary palate reveal continuous mesenchyme between the maxillary prominence and the frontonasal mass (c–d′). ant, anterior; e, eye; fnm, frontonasal mass; lat, lateral; lnp, lateral nasal prominence; med, medial; mnp; medial nasal prominence; mxp, maxillary prominence; nc, nasal cavity; pos, posterior; s, stomodeum

the external nares become reduced in size to small openings (Figure 2b,b′—red arrow), and complete closure occurs shortly thereafter. In order to better understand the epithelial–mesenchymal interaction during this process, we compared the newly identified nasal cavity fusion zone to the well-studied fusion of the primary palate/upper jaw in stage 29 animals (Figure 3). Cross-sections in the transverse plane show retained epithelium between the medial nasal and lateral nasal prominences after closure of the nasal cavity (Figure 3a-b′—red arrowhead). In contrast, the fusion zone between the maxillary prominence and the frontonasal mass (primary palate fusion) exhibited continuous mesenchyme, which indicates the breakdown of the intervening epithelium (commonly referred to as the nasal fin) (Figure 3c-d′).

3.2 Phase 2: extent of nasal plug and interaction with the nasal conchae (stages 34–38)

At stage 34 (Figure 4a), a coronal section of the beak reveals obstruction of the nasal vestibule at the level of the external nares (Figure 4b). In the section immediately posterior to the nares, the developing rostral concha is visible as delineation within the tissue comprising the nasal plug (Figure 4c). Further posterior, the middle nasal and caudal nasal conchae are also apparent at this stage, but in the form of outgrowths from the lateral nasal walls into the respiratory and olfactory portions of the nasal cavity, posterior to the nasal vestibule (Figure 4d). Stage 38 specimens were also analyzed in a similar manner (Figure 4e), and reveal more extensive rostral conchae within the nasal plug (Figure 4f). A transverse view of a stage 38 embryo reveals that the nasal plug is limited to the nasal vestibule, while the posterior nasal cavity remains free of obstruction, as evidenced by the darker color of the patent cavity space (Figure 4g′—white arrowhead). Furthermore, the relative positions of the nasal conchae are confirmed in the transverse view, with the rostral conchae developing within the plug tissue in the anterior vestibule and the middle and caudal conchae developing within the patent posterior nasal cavity (Figure 4g,g′).

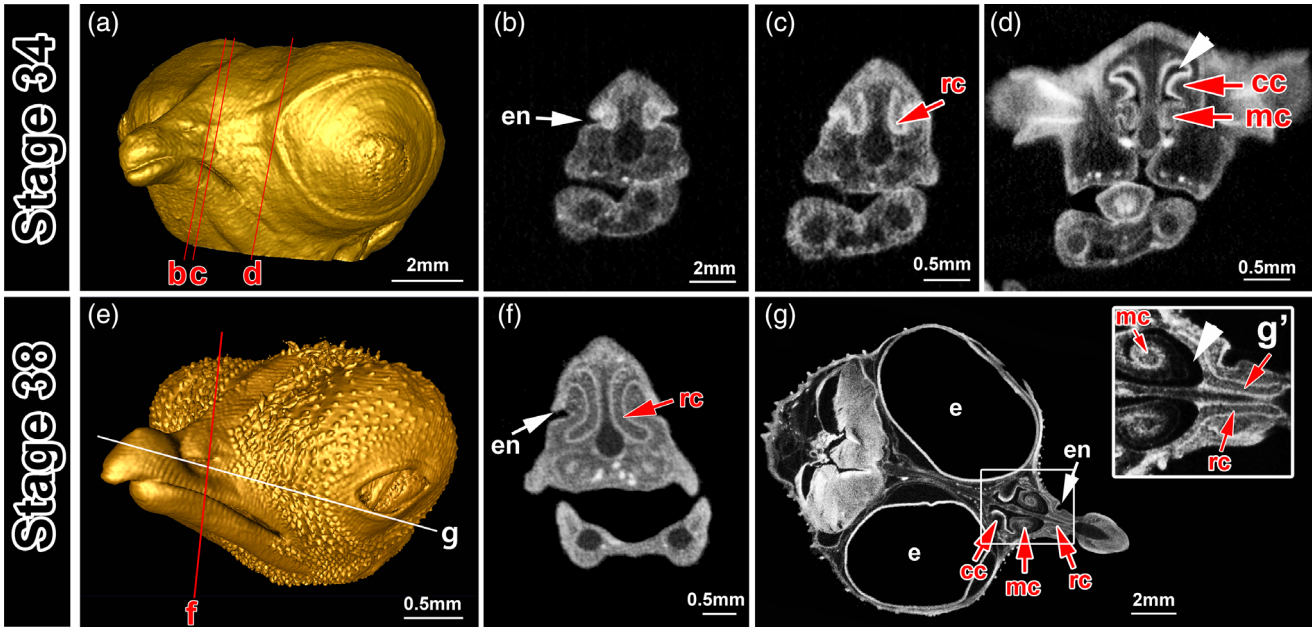

Fig. 4. MicroCT slices through the beaks of stage 34 and stage 38 embryos reveal persistent occlusion of the nasal vestibule. Coronal slices through stage 34 embryo (a) reveal occlusion of the external naris (b) and the beginning of rostral concha formation (c). Further posterior slice reveals outgrowth of the middle and caudal conchae into the nasal cavity (d), which looks patent based on darker shading. A stage 38 specimen (e) reveals more advanced rostral conchae (f). Section in the transverse plane confirms that the nasal plug is restricted to the nasal vestibule, whereas the nasal cavity proper appears patent (g, g′-white arrowhead). cc, caudal nasal conchae; en, external naris; mc, middle nasal conchae; rc, rostral nasal conchae

3.3 Phase 3: recanalization of the nasal cavity (stages 39–44)

Histological analysis of stage 39–44 embryos revealed the progressive breakdown of the cells encapsulated within the nasal vestibule. At stages 39 and 40, the nasal cavities exhibit uniform concentration of epithelial cells continuous with the epithelium of the nasal wall and alinasal folds (Figure 5a,b′). Beginning with stage 41, the cells at the center of the epithelial plug appear to expand, as evidenced by larger cytoplasmic area and lighter staining (Figure 5c,c′). Subsequent stages reveal progressive expansion of the central cells, eventually leading to their rupture and complete canalization by stage 44 in all embryos examined (Figure 5d–f′). Some embryos did exhibit partial canalization as early as stage 42 but not earlier (data not shown). Closer inspection of the cells at the putative opening of the external naris revealed stretching of the cells across the nasal cavity (Figure 5g), eventually tearing apart during the recanalization process (Figure 5h).

Since picrosirius red staining did not sufficiently resolve the position of cells along the edges of the nasal plug, we decided to apply DAPI nuclear staining to sections equivalent to those of the histological preparations (illustrated in Figure 6a). DAPI staining confirmed the widening of the nasal vestibule, with the center exhibiting less nuclear signal as fewer, more expanded cells occupy that space. The cells closer to the edges of the nasal vestibule intercalate and stack into organized columns along the walls. This behavior may be observed as early as stages 39–40 in some cells (Figure 6b,c), continuing into stage 41, and reaching its most-organized state at stage 42 (Figure 6d,e). Columns then begin breaking down by stage 43 (Figure 6f). Due to the apparent breakdown of cell columns at stage 43, stage 41–43 specimens were tested for apoptotic signals using a TUNEL assay. Stage 41 specimens exhibited no TUNEL signal (Figure 7a), while stage 42 specimens revealed signal along the walls of the nasal vestibule (Figure 7b). By stage 43, the signal is once again lost (Figure 7c). A magnified view of stage 42 revealed a very strong and specific signal within the intercalated cellular columns lining the walls of the primitive nasal cavity (Figure 7d–f).

4. DISCUSSION

Among the reptilian relatives of birds, the formation of a cellular nasal plug has been described in the tuatara embryo (*Sphenodon punctatus*) (Howes & Swinnerton, 1901), as well as the African rock python (*Python sebae*) (Buchtova et al., 2007). While Howes and Swinnerton (1901) do not describe the exact stages of nasal plug formation and breakdown in tuatara, the python appears to exhibit a similar period of nasal vestibule occlusion when compared to chicken (Figure 8). Additionally, Abramyan et al. (2015) have previously described fusion between the lateral nasal and medial nasal prominences, similar to chicken, in embryonic stages of three lizard species: *Aspidoscelis uniparens* (Teiidae) at stage 12, *Pogona vitticeps* (Agamidae) stage 31, and *Chamaeleo calyptratus* (Chamaeleonidae) at stage 34 (see Abramyan et al., 2015 for staging methods used). The fact that this process was identified across such distantly related species suggests that it is part of normal lacertilian embryonic development. Unfortunately, limited sample availability precluded the study of later stages to detect whether the epithelial

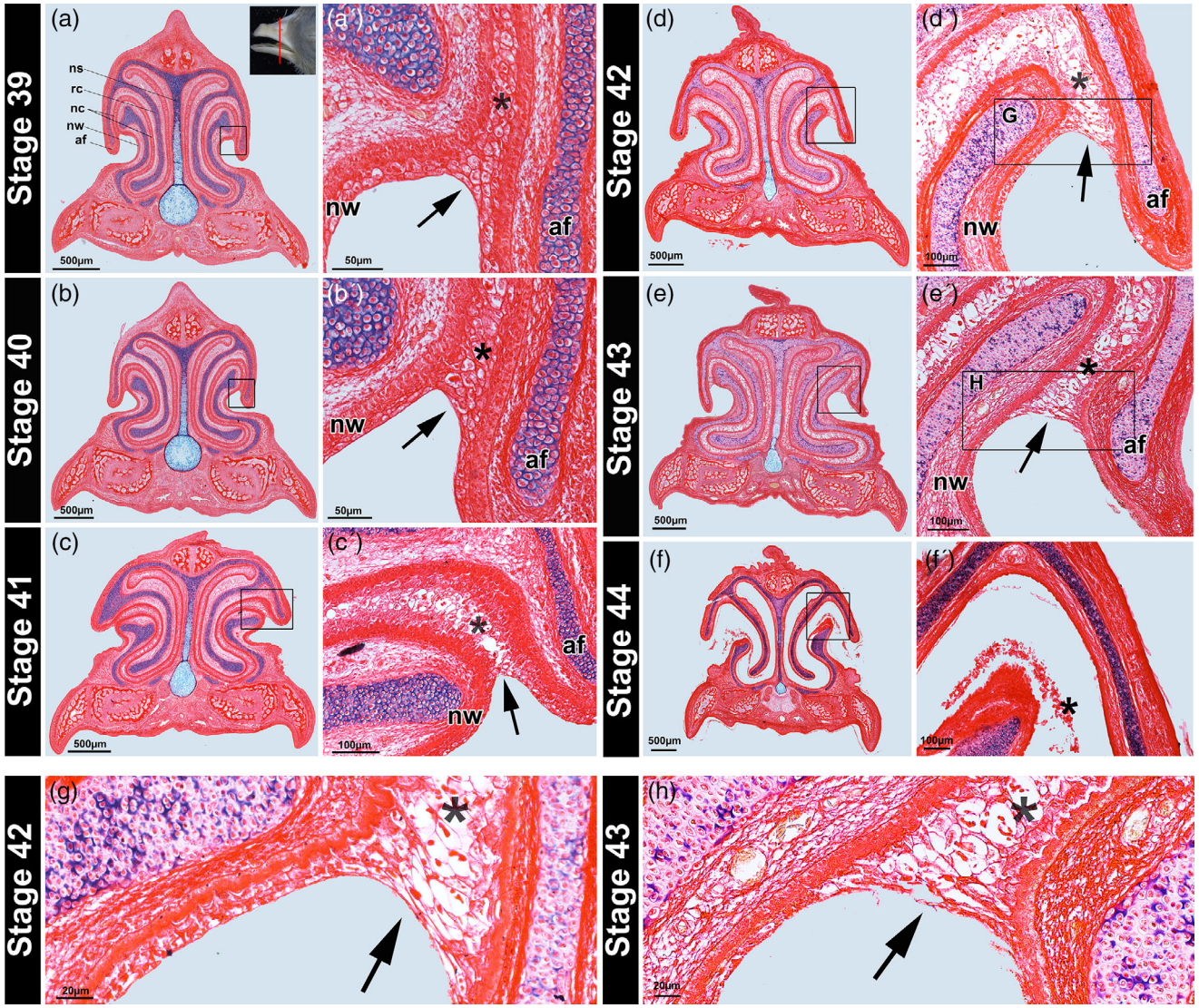

Fig. 5. Recanalization of the nasal vestibule observed through histological sections in the coronal plane. In specimens ranging from stage 39 to 43, the external naris is obstructed by cells of the nasal plug, which are continuous with the epithelium covering the nasal wall and alinasal fold (arrow) (a–e′). Beginning from stage 41, specimens exhibit the expansion of the cells in the center of the nasal plug (asterisk) (c–e′). Complete recanalization of the nasal vestibule was observed in all stage 44 specimens (f, f′). Magnified views of stage 42 and 43 specimens reveal the stretched appearance of cells at the opening of the external naris (g), before they rupture during the recanalization process (h). af, alinasal fold; nc, nasal cavity; ns, nasal septum; nw, nasal wall; rc, rostral nasal concha

seams between the fused prominences go on to form a more substantial nasal plug in lizards as they do in chicken and snake. While crocodilian and testudine embryos remain to be described, the studies cited above, in conjunction with the work presented in this article, suggest that nasal plug formation may be a shared developmental characteristic across sauropsids.

Description of nasal plugs in mammalian embryos goes back to studies on humans published in the early 1900s (Schaeffer, 1910). Since then very few studies have described the mammalian nasal plugs in nonhuman embryos, with available information limited to studies of rabbit (Alomaisi et al., 2018), baboon (Bollert & Hendrickx, 1971), and mouse (Rugh, 1968) (Figure 8). Recently, more detailed studies of human embryos have described the plug as developing between the 8th week of gestation (Carnegie stage 20) (Kim et al., 2004; Yoon et al., 2000) and the 10th week (Nishimura, 1993). Recanalization is then thought to occur between the 13th and 17th weeks of gestation (Kim *et al.*, 2016), with some studies suggesting retention of the plug till the 22nd week (Diewert & Shiota, 1990) or even 24th week (Kumoi et al., 1993; Sarnat & Yu, 2016) (Figure 8). Taken from the limited data that are available, comparative analysis of nasal plug formation reveals an earlier loss of nasal plugs in mammalian embryos in comparison to sauropsid lineages (Figure 8). However, further studies are required to establish more definite stages of nasal plug formation and breakdown, both in humans as well as other mammals.

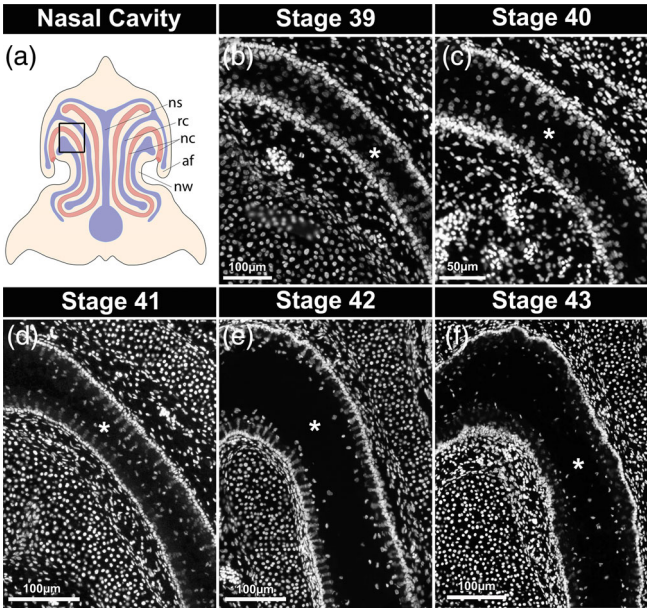

Fig. 6. DAPI staining was performed on histological sections of the embryonic beak in the coronal plane, as illustrated in panel (a). Stained sections reveal progressive loss of nuclear signal through stages 39–43. At stage 39, the nasal plug is intact and reveals a relatively uniform signal in the center of the nasal vestibule (b). By stage 40, the signal is slightly reduced in the center and the cells along the edges exhibit some intercalation and stacking (c). Around stages 41–42, signal in the center is further reduced, while cells along the edges become highly organized into columns (d, e). At stage 43, columns appear to lose their organization (f). af, alinasal fold; af, alinasal fold; nc, nasal cavity; ns, nasal septum; nw, nasal wall; rc, rostral nasal concha

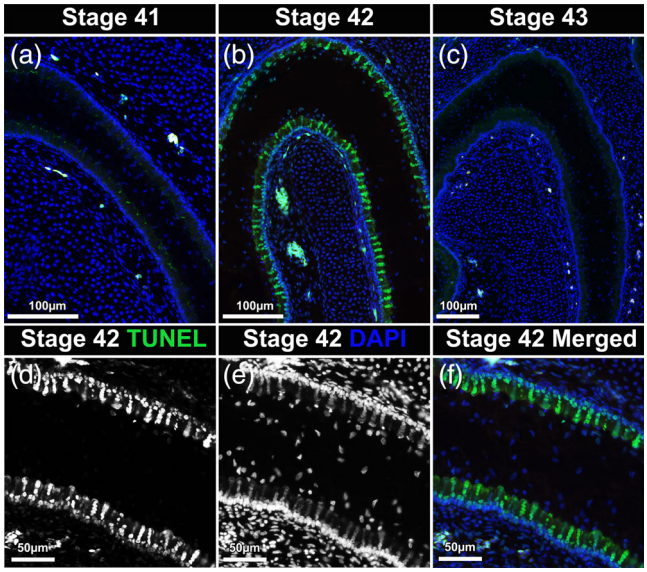

Fig. 7. TUNEL analysis for apoptotic activity applied to stage 41–43 specimens. Stage 41 exhibits little to no TUNEL signal (green) as compared to background DAPI stained cells (blue) (a). At stage 42, TUNEL-positive cells become apparent along the walls of the nasal vestibule (b), with signal disappearing by stage 43 (c). Closer examination of stage 42 specimen TUNEL-positive region (d), in comparison to DAPI staining (e), reveals localization of TUNEL signal to cells that make up the columns lining the walls of the primitive nasal vestibule (f)

Additionally, the nasal plugs in the human embryo are described as occurring in the "anterior" region of the nasal cavity (Diewert & Shiota, 1990; Kim et al., 2004; Kim *et al*., 2016), similar to the chicken nasal plug being limited to the nasal vestibule. This similarity may inform us about the role of the plugs in the respective species, as well as furthering our understanding of nasal cavity compartmentalization and evolution in amniotes. That said, there do seem to be differences between human nasal plugs and the structure we describe in chicken. Photomicrographs of human nasal plugs in several independent studies appear to show discontinuity between the epithelial plug and the epithelium lining the nasal vestibule (Diewert & Shiota, 1990; Humphrey, 1969; Schaeffer, 1910), while in the chicken, we show that the epithelial cells of the nasal plug are continuous with those of the nasal vestibule and even the craniofacial prominences. Therefore, these structures may be convergent in humans and birds and may warrant different nomenclature.

4.1 Recanalization of the nasal vestibule

Very few studies have addressed the cellular mechanism underlying the recanalization of the nasal vestibule (Masumoto et al., 2010). Schaeffer (1910) initially suggested that human nasal plugs are physically shed rather than broken down. Indeed, since the nasal plugs appear to be physically disconnected from the craniofacial epithelium, as noted earlier, this may be the case in humans but is not so in chicken. Furthermore, in a study of human fetus at 15 weeks, Masumoto et al. (2010) state that the nasal cavity is negative for TUNEL immunoreactivity. However, close inspection of the image presented in their study does appear to show some signal in the walls of the nasal plug, albeit less organized than what we observed in chicken. Therefore, further investigation of apoptosis in the human nasal plug is certainly warranted, especially given our results.

4.2 Nasal concha formation within the nasal plug

The avian rostral conchae are morphologically and functionally analogous to the mammalian maxilloturbinals, although they are thought to have arisen independently in each group during their transition into endothermy (Hillenius, 1992; Hillenius & Ruben, 2004; Parsons, 1967; Ruben, Jones, & Geist, 1998; Witmer, 1995). Our results show that in the avian embryo, the rostral concha grows within the tissue comprising the nasal plug, which then breaks down around it. In mammals, this process is less well understood. At first glance, it would appear that mammals experience direct outgrowth of conchae from the nasal wall into a patent nasal vestibule (Smith & Rossie, 2008; Van Valkenburgh et al., 2014), including in humans (Bingham, Wang, Hawke, & Kwok, 1991; Wake, Takeno, & Hawke, 1994; Wang & Jiang, 1997). However, the human literature (which is the most extensive) on nasal plug and nasal turbinal development reveals an overlap in the timing of development of these two structures. In describing the developing

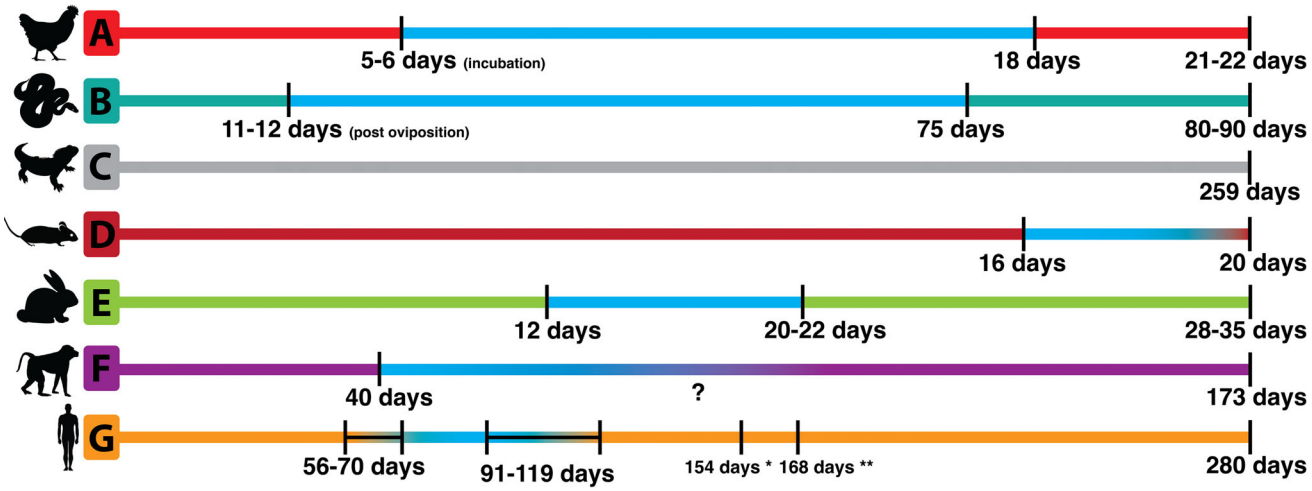

Fig. 8. Scaled comparison of nasal plug formation and loss across amniote taxa relative to their respective total incubation periods. Chicken (*Gallus gallus*) (Hamburger & Hamilton, 1951) and python (*Python sebae*) (Boughner et al., 2007; Buchtova et al., 2007) exhibit similar period of nasal plug retention (a, b). In the tuatara (*Sphenodon punctatus*), Howes and Swinnerton (1901) do not describe the timing of nasal plug formation, but simply state that they are resorbed shortly before hatching (at 259 days—Thompson, 1990) (c). In the mouse (*Mus musculus*), the nasal plug is observed at E16, but loss is described as being prior to birth (Rugh, 1968) (d). In the rabbit (*Oryctolagus cuniculus*), nasal plugs form at 12 days and breaks down at 20–22 days (Alomaisi et al., 2018) (e). In baboon (*Papio cynocephalus*), nasal plugs are observed at 40 days (Stage XIX—16.3 mm), but loss prior birth is not recorded (Bollert & Hendrickx, 1971) (173 day gestation period—Albrecht & Townsley, 1978) (f). In humans, formation of the nasal plug occurs at 56–70 days (8–10 weeks) (Kim et al., 2004; Nishimura, 1993; Yoon, Chung, Seol, Park, & Park, 2000), while various dates are recorded for the period of nasal plug loss, ranging from 91–119 days (Kim *et al*., 2016), to 154 days (Diewert & Shiota, 1990) and 168 days (Kumoi, Nishimura, & Shiota, 1993; Sarnat & Yu, 2016)

human maxilloturbinals, several studies describe the nasal turbinals in 8-week-old embryos, with no mention of a nasal plugs (Bingham et al., 1991; Müller & O'Rahilly, 2004; Neskey, Eloy, & Casiano, 2009; Wake et al., 1994; Wang & Jiang, 1997). On the other hand, studies focusing on nasal plugs describe them as forming at the same developmental time points (Carnegie stage 20, ~8 weeks of gestation) with no mention of the nasal turbinals (Diewert & Shiota, 1990; Kim et al., 2004; Yoon et al., 2000). This disparity may be due to misstaging of embryos or positional differences between histological sections. Therefore, it remains unknown whether mammalian maxilloturbinals also develop within the nasal plug or not.

5. CONCLUSIONS

In this study, we describe a developmental process that has gone unnoticed in the chicken embryo: the development of a nasal plug. The obstruction and subsequent recanalization of embryonic nasal cavities may at first seem like a counterintuitive developmental step, and yet is observed repeatedly across diverse amniote lineages. Despite the seeming ubiquity of epithelial obstructions in embryonic cavities, there is little in the way of hypotheses in the current literature for their existence. Furthermore, while the nasal plugs have been recognized in embryological studies, few studies describe the cellular processes involved in their development and subsequent breakdown, with some conflicting ideas of whether they are extruded or undergo cellular breakdown within the cavity. In working with the chicken embryo, we have advanced the knowledge of these structures further by not only describing their formation but also the cellular breakdown involved in recanalization. Through this study, we hope to pave the way for further research of these tissues across taxa, thereby filling this gap in the knowledge of amniote developmental biology.

ACKNOWLEDGMENTS

We would like to thank Michelle Lynch for assistance with microCT scan optimization. Specimens were scanned at the University of Michigan School of Dentistry MicroCT Core funded in part by NIH/NCRR S10RR026475-01. J.A. is a member of the Michigan Integrative Musculoskeletal Health Core Center (MiMHC) and as such, research reported in this publication was supported by the National Institute of Arthritis and Musculoskeletal and Skin Diseases of the National Institutes of Health under Award Number P30 AR069620. The content is solely the responsibility of the authors and does not necessarily represent the official views of the National Institutes of Health. Funding was also provided by Undergraduate Student Independent Research Grant from the University of Michigan-Dearborn to Z.A. and startup funds from the University of Michigan-Dearborn to J.A. Lastly, we would like to thank the reviewers whose suggestions greatly improved our manuscript.

CONFLICT OF INTEREST

The authors declare no potential conflict of interest.

AUTHOR CONTRIBUTIONS

Zahra Albawaneh and Raana Ali contributed equally to this work. Zahra Albawaneh was responsible for microCT segmentation, histology, and drafting of the manuscript. Raana Ali was responsible for data interpretation,

histology, and constructive review of the manuscript. John Abramyan was responsible for project design, figure preparation, and drafting of the manuscript.

REFERENCES

Abramyan, J., & Richman, J. M. (2015). Recent insights into the morphological diversity in the amniote primary and secondary palates. Developmental Dynamics, 244, 1457–1468.

Abramyan, J., & Richman, J. M. (2018). Craniofacial development: Discoveries made in the chicken embryo. The International Journal of Developmental Biology, 62, 97–107.

Abramyan, J., Thivichon-Prince, B., & Richman, J. M. (2015). Diversity in primary palate ontogeny of amniotes revealed with 3D imaging. Journal of Anatomy, 226, 420–433.

Albrecht, E. D., & Townsley, J. D. (1978). Serum estradiol in mid and late gestation and estradiol/progesterone ratio in baboons near parturition. Biology of Reproduction, 18, 247–250.

Alomaisi, S. A., El-Ghazali, H. M., Nosseur, H. M., Ahmed, S. E. D. A., & Konsowa, M. M. (2018). Prenatal development of the nostril in rabbit (Orycmtolagus cuniculus). Journal of Veterinary Anatomy, 11, 57–68.

Bedell, M. A., Jenkins, N. A., & Copeland, N. G. (1997). Mouse models of human disease. Part I: Techniques and resources for genetic analysis in mice. Genes & Development, 11, 1–10.

Bedell, M. A., Largaespada, D. A., Jenkins, N. A., & Copeland, N. G. (1997). Mouse models of human disease. Part II: Recent progress and future directions. Genes & Development, 11, 11–43.

Bingham, B., Wang, R. G., Hawke, M., & Kwok, P. (1991). The embryonic development of the lateral nasal wall from 8 to 24 weeks. Laryngoscope, 101, 992–997.

Bollert, J. A., & Hendrickx, A. G. (1971). Morphogenesis of the palate in the baboon (Papio cynocephalus). Teratology, 4, 343–353.

Boughner, J. C., Buchtova, M., Fu, K., Diewert, V., Hallgrimsson, B., & Richman, J. M. (2007). Embryonic development of *Python sebae* - I: Staging criteria and macroscopic skeletal morphogenesis of the head and limbs. Zoology, 110, 212–230.

Buchtova, M., Boughner, J. C., Fu, K., Diewert, V. M., & Richman, J. M. (2007). Embryonic development of *Python sebae* - II: Craniofacial microscopic anatomy, cell proliferation and apoptosis. Zoology, 110, 231–251.

Craven, B. A., Neuberger, T., Paterson, E. G., Webb, A. G., Josephson, E. M., Morrison, E. E., & Settles, G. S. (2007). Reconstruction and morphometric analysis of the nasal airway of the dog (*Canis familiaris*) and implications regarding olfactory airflow. The Anatomical Record, 290, 1325–1340.

Dahl, R., & Mygind, N. (1998). Mechanisms of airflow limitation in the nose and lungs. Clinical and Experimental Allergy, 2, 17–25.

Diewert, V. M., & Shiota, K. (1990). Morphological observations in normal primary palate and cleft lip embryos in the Kyoto collection. Teratology, 41, 663–677.

Dodgson, J. B., & Romanov, M. N. (2004). Use of chicken models for the analysis of human disease. Current Protocols in Human Genetics, 15, 15.5.

Gignac, P. M., Kley, N. J., Clarke, J. A., Colbert, M. W., Morhardt, A. C., Cerio, D., … Witmer, L. M. (2016). Diffusible iodine-based contrast-enhanced computed tomography (diceCT): An emerging tool for rapid, high-resolution, 3-D imaging of metazoan soft tissues. Journal of Anatomy, 228, 889–909.

Hamburger, V., & Hamilton, H. L. (1951). A series of normal stages in the development of the chick embryo. Journal of Morphology, 88, 49–92.

Hillenius, W. J. (1992). The evolution of nasal turbinates and mammalian endothermy. Paleobiology, 18, 17–29.

Hillenius, W. J. (1994). Turbinates in Therapsids: Evidence for late permian origins of mammalian endothermy. Evolution, 48, 207–229.

Hillenius, W. J., & Ruben, J. A. (2004). The evolution of endothermy in terrestrial vertebrates: Who? When? Why? Physiological and Biochemical Zoology, 77, 1019–1042.

Howes, G. B., & Swinnerton, H. H. (1901). On the development of the skeleton of the tuatara, *Sphenodon punctatus*; with remarks on the egg, on the hatching, and on the hatched young. Transactions of the Zoological Society of London, 16, 1–84.

Humphrey, T. (1969). The relation between human fetal mouth opening reflexes and closure of the palate. Journal of Anatomy, 125, 317–344.

Jankowski, R. (2011). Revisiting human nose anatomy: Phylogenic and ontogenic perspectives. Laryngoscope, 121, 2461–2467.

Jiang, R., Bush, J. O., & Lidral, A. C. (2006). Development of the upper lip: Morphogenetic and molecular mechanisms. Developmental Dynamics, 235, 1152–1166.

Kain, K. H., Miller, J. W., Jones-Paris, C. R., Thomason, R. T., Lewis, J. D., Bader, D. M., … Zijlstra, A. (2014). The chick embryo as an expanding experimental model for cancer and cardiovascular research. Developmental Dynamics, 243, 216–228.

Kim, C. H., Park, H. W., Kim, K., & Yoon, J. H. (2004). Early development of the nose in human embryos: A stereomicroscopic and histologic analysis. Laryngoscope, 114, 1791–1800.

Kim, J. H., Jin, Z. W., Murakami, G., & Cho, B. H. (2016). Characterization of mesenchymal cells beneath cornification of the fetal epithelium and epidermis at the face: an immunohistochemical study using human fetal specimens. Anatomy & cell biology, 49, 50-60.

Kumoi, T., Nishimura, Y., & Shiota, K. (1993). The embryologic development of the human anterior nasal aperture. Acta Oto-Laryngologica, 113, 93–97.

Kurosaka, H. (2019). Choanal atresia and stenosis: Development and diseases of the nasal cavity. Wiley Interdisciplinary Reviews: Developmental Biology, 8, e336.

Masumoto, H., Katori, Y., Kawase, T., Cho, B. H., Murakami, G., Shibata, S., & Matsubara, A. (2010). False positive reactivity of a substance P-antibody in the ectodermal/epithelial plug of the nose, ear, eye and perineum of the human and mouse fetuses. Okajimas Folia Anatomica Japonica, 87, 33–40.

Müller, F., & O'Rahilly, R. (2004). Olfactory structures in staged human embryos. Cells, Tissues, Organs, 178, 93–116.

Neskey, D., Eloy, J. A., & Casiano, R. R. (2009). Nasal, septal, and turbinate anatomy and embryology. Otolaryngologic Clinics of North America, 42, 193–205.

Nishimura, Y. (1993). Embryological study of nasal cavity development in human embryos with reference to congenital nostril atresia. Acta Anatomica, 147, 140–144.

Parsons, T. E. (1959). Studies on the comparative embryology of the reptilian nose. Bulletin of the Museum of Comparative Zoology at Harvard College, 120, 101–277.

Parsons, T. S. (1967). Evolution of the nasal structure in the lower tetrapods. American Zoologist, 7, 397–413.

Parsons, T. S. (1970). The nose and Jacobsons's organ. In C. Gans (Ed.), *Biology of reptilia, Vol. 2 (Morphology B)* (pp. 99–199). New York, NY: Academic Press.

Richman, J. M., & Tickle, C. (1989). Epithelia are interchangeable between facial primordia of chick embryos and morphogenesis is controlled by the mesenchyme. Developmental Biology, 136, 201–210.

Rossie, J. B. (2006). Ontogeny and homology of the paranasal sinuses in Platyrrhini (Mammalia: Primates). Journal of Morphology, 267, 1–40.

Rowe, T. B., Eiting, T. P., Macrini, T. E., & Ketcham, R. A. (2005). Organization of the olfactory and respiratory skeleton in the nose of the gray short-tailed opossum *Monodelphis domestica*. Journal of Mammalian Evolution, 12, 303–336.

Ruben, J. A., Jones, T. D., & Geist, N. R. (1998). Respiratory physiology of the dinosaurs. BioEssays, 20, 852–859.

Rugh, R. (1968). *The mouse. Its reproduction and development*. Minneapolis, MN: Burgess Pub. Co.

Sarnat, H. B., & Yu, W. (2016). Maturation and dysgenesis of the human olfactory bulb. Brain Pathology, 26, 301–318.

Schaeffer, J. P. (1910). The lateral wall of the cavum nasi in man, with especial reference to the various developmental stages. Journal of Morphology, 21, 613–707.

Smith, T. D., & Rossie, J. B. (2008). Nasal fossa of mouse and dwarf lemurs (primates, cheirogaleidae). The Anatomical Record, 291, 895–915.

Tamarin, A., Crawley, A., Lee, J., & Tickle, C. (1984). Analysis of upper beak defects in chicken embryos following with retinoic acid. Journal of Embryology and Experimental Morphology, 84, 105–123.

Thompson, M. B. (1990). Incubation of eggs of tuatara, *Sphenodon punctatus*. Journal of Zoology, 222, 303–318.

Van Valkenburgh, B., Smith, T. D., & Craven, B. A. (2014). Tour of a labyrinth: Exploring the vertebrate nose. The Anatomical Record, 297, 1975–1984.

Wake, M., Takeno, S., & Hawke, M. (1994). The early development of sino-nasal mucosa. Laryngoscope, 104, 850–855.

Wang, R. G., & Jiang, S. C. (1997). The embryonic development of the human ethmoid labyrinth from 8-40 weeks. Acta Oto-Laryngologica, 117, 118–122.

Wassif, C. A., Zhu, P., Kratz, L., Krakowiak, P. A., Battaile, K. P., Weight, F. F., … Porter, F. D. (2001). Biochemical, phenotypic and neurophysiological characterization of a genetic mouse model of RSH/Smith–Lemli–Opitz syndrome. Human Molecular Genetics, 10, 555–564.

Wedden, S. E. (1987). Epithelial-mesenchymal interactions in the development of chick facial primordia and the target of retinoid action. Development, 99, 341–351.

Will, L. A., & Meller, S. M. (1981). Primary palatal development in the chick. Journal of Morphology, 169, 185–190.

Witmer, L. M. (1995). Homology of facial structures in extant archosaurs (birds and crocodilians), with special reference to paranasal pneumaticity and nasal conchae. Journal of Morphology, 225, 269–327.

Yee, G. W., & Abbott, U. K. (1978). Facial development in normal and mutant chick embryos. I. Scanning electron microscopy of primary palate formation. The Journal of Experimental Zoology, 206, 307–321.

Yoon, H., Chung, I. S., Seol, E. Y., Park, B. Y., & Park, H. W. (2000). Development of the lip and palate in staged human embryos and early fetuses. Yonsei Medical Journal, 41, 477–484.